The G473D Mutation Impairs Dimerization and Catalysis in Human Sulfite Oxidase†

Heather L. Wilson, Sara R. Wilkinson, and K. V. Rajagopalan*

Department of Biochemistry, Box 3711, Duke University Medical Center, Durham, North Carolina 27710

Received August 12, 2005; Revised Manuscript Received December 12, 2005

ABSTRACT: Among the mutations identified in patients with isolated sulfite oxidase deficiency, the G473D variant is of particular interest since sedimentation analysis reveals that this variant is a monomer, and the importance of the wild-type dimeric state of mammalian sulfite oxidase is not yet well understood. Analysis of recombinant G473D sulfite oxidase indicated that it is severely impaired both in the ability to bind sulfite and in catalysis, with a second-order rate constant 5 orders of magnitude lower than that of the wild type. To elucidate the specific reasons for the severe effects seen in the G473D variant, several other variants were created, including G473A, G473W, and the double mutant R212A/G473D. Despite the inability to form a stable dimer, the G473W variant had 5-fold higher activity than G473D and nearly wild-type activity at pH 7.0 when ferricyanide was the electron acceptor. In contrast, the R212A/G473D variant demonstrated some ability to oligomerize but had undetectable activity. The G473A variant retained the ability to dimerize and had steady-state activity that was comparable to that of the wild type. Furthermore, stopped-flow analysis of the reductive half-reaction of this variant yielded a rate constant nearly 3 times higher than that of the wild type. Examination of the secondary structures of the variants by CD spectroscopy indicated significant random-coil formation in G473D, G473W, and R212A/G473D. These results demonstrate that both the charge and the large size of an Asp residue in this position contribute to the severe effects seen in a patient with the G473D mutation, by causing partial misfolding and monomerization of sulfite oxidase and attenuating both substrate binding and catalytic efficiency during the reaction cycle.

Mammalian sulfite oxidase (SO,[1] EC 1.8.3.1) is the signature member of the family of proteins containing the form of the molybdenum cofactor that consists of a single molybdenum atom coordinated through the dithiolene group of a single molybdopterin (MPT) molecule (*1*, *2*). Other members of the SO superfamily include plant SO (*3*), assimilatory nitrate reductase (*4*), and bacterial sulfite dehydrogenase (SDH) (*5*). Mammalian SO resides in the mitochondrial intermembrane space and performs the final step in the oxidative degradation of the amino acids methionine and cysteine as well as other sulfur-containing compounds (including toxic metabolites) by oxidizing sulfite to sulfate in the reaction shown here (*1*, *6*, *7*).

$$SO_3^{2-} + H_2O + 2(\text{cyt } c)_{ox} \rightarrow SO_4^{2-} + 2(\text{cyt } c)_{red} + 2H^+ \quad (1)$$

Both human and rat SO have been cloned, recombinantly expressed in *Escherichia coli*, and purified (*8*−*10*), and the crystal structure of chicken liver SO has been determined at a resolution of 1.9 Å (*11*). Each 55 kDa subunit of chicken SO includes N- and C-terminal domains linked by a hinge region that was not resolved in the crystal structure and is thus presumed to be flexible (*11*). The 10 kDa N-terminal portion (heme domain) of each subunit contains a b_5-type heme that is deeply buried but not covalently attached to the protein. The 42 kDa C-terminal region (Mo domain) can be further divided into two subdomains: the MPT-binding region and the dimerization interface (Figure 1A). The 10 kDa heme domain of SO can be removed by trypsin cleavage at the flexible hinge region, and the remaining C-terminal Mo domain retains both the MPT cofactor and the ability to dimerize (*12*). In addition, the Mo domain can oxidize sulfite in the presence of a nonspecific electron acceptor such as ferricyanide (*12*).

The overall SO reaction cycle (Figure 2) can be divided into reductive and oxidative half-reactions (*7*). In the reductive half of the reaction cycle, sulfite binds at the Mo^{VI} center and is oxidized to sulfate, yielding the two-electron reduced $Mo^{IV}Fe^{III}$ species of SO. In full-length SO, this species cannot be observed due to its transient nature and the spectral interference of the heme Fe. However, stopped-flow analysis has been used to monitor and obtain a rate constant for this reaction (k_{red}^{Mo}) using the isolated Mo domain (*13*). In the first intramolecular electron transfer (IET #1, Figure 2), one electron is transferred from Mo^{IV} to the

† This work was supported by Grant GM44283 to K.V.R. from the National Institutes of Health.

* To whom correspondence should be addressed: Department of Biochemistry, Box 3711, Duke University Medical Center, Durham, NC 27710. Telephone: (919) 681-8845. Fax: (919) 684-8919. E-mail: raj@biochem.duke.edu.

[1] Abbreviations: Bis-Tris, bis(2-hydroxyethyl)aminotris(hydroxymethyl)methane; Bis-Tris propane, 1,3-bis[tris(hydroxymethyl)methylamino]propane; cyt *c*, cytochrome *c*; EDTA, ethylenediaminetetraacetic acid; ELDOR, electron−electron double resonance; EPR, electron paramagnetic resonance; EXAFS, extended X-ray absorption fine structure; HPLC, high-performance liquid chromatography; IET, intramolecular electron transfer; MPT, molybdopterin; Tris, tris(hydroxymethyl)aminomethane; SDH, bacterial sulfite dehydrogenase; SO, sulfite oxidase.

10.1021/bi051609l CCC: $33.50
Published on Web 01/25/2006

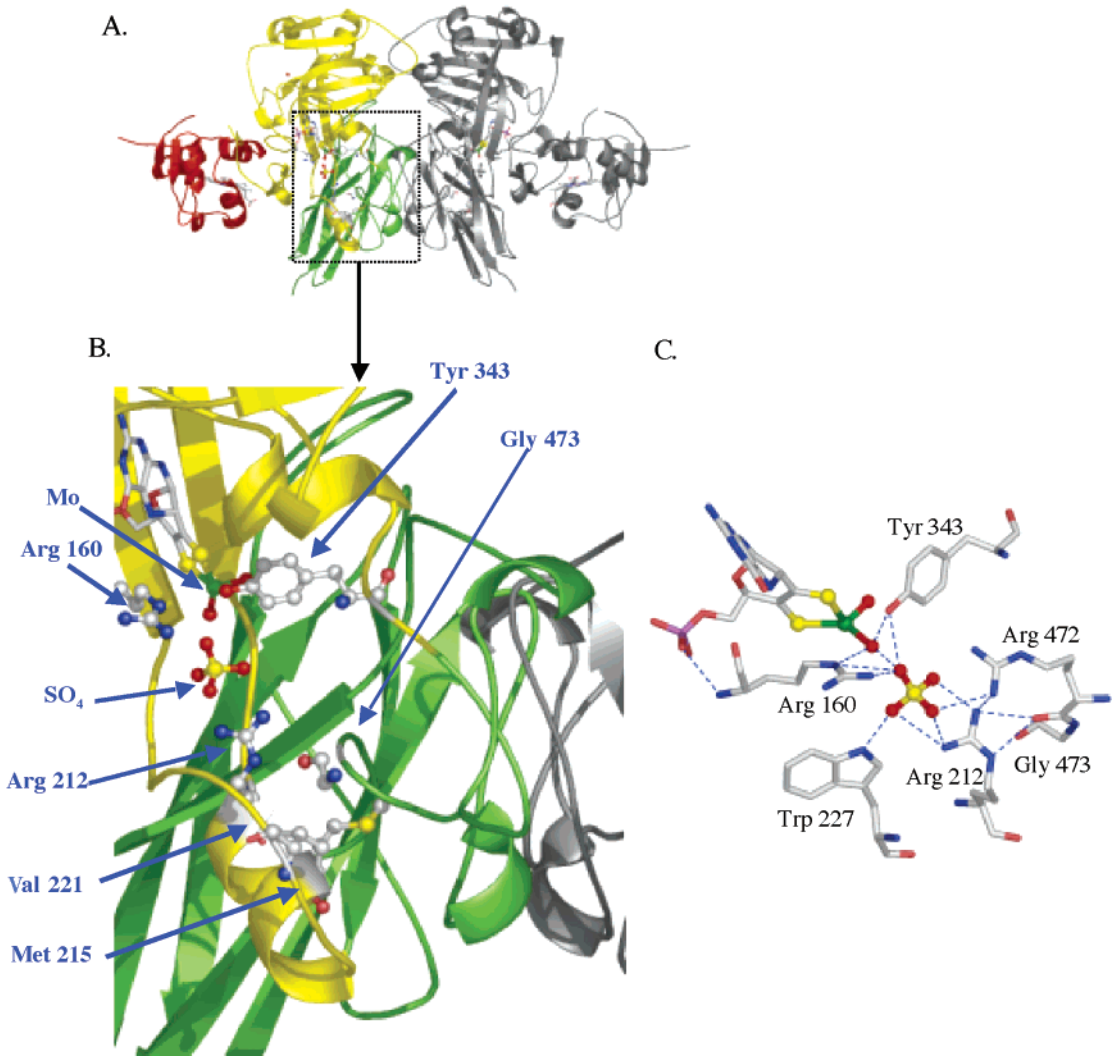

FIGURE 1: (A) Crystal structure of chicken SO. The heme domain of one monomer is colored red (residues 3−84), the MPT-binding domain yellow (residues 96−323), and the dimerization interface (residues 324−466) green. The second monomer is colored gray. (B) Structure of the region around Gly 451 (Gly 473 in human). The Mo cofactor, the sulfate molecule, and the Arg 160, Arg 212, Val 221, Tyr 343, and Gly 473 residues (human numbering) are shown in ball-and-stick format. (C) Active site of chicken SO. The Mo atom is colored green; S atoms are colored yellow, O atoms red, and N atoms cyan. The PyMOL Molecular Graphics Program (*48*) was used to create this figure from the atomic coordinates of the crystal structure of chicken SO (*11*) deposited in the Molecular Modeling Database as entry 7838 (http://www.ncbi.nlm.nih.gov:80/Structure/MMDB/mmdb.shtml).

heme in the N-terminus of SO to yield a $Mo^{V}Fe^{II}$ species that can be detected using electron paramagnetic resonance (EPR) spectroscopy (*14*−*17*). The rate constant of the reductive half-reaction (k_{red}^{heme}) has been determined using stopped-flow analysis by directly monitoring the reduction of the heme from Fe^{III} to Fe^{II} at 425 nm (*13*, *18*, *19*). The oxidative half of the reaction cycle begins when one electron is transferred from Fe^{II} to the exogenous terminal electron acceptor, cyt *c*. After a second IET from Mo^{V} to Fe^{III} to produce the $Mo^{VI}Fe^{II}$ state of the enzyme, the protein returns to the fully oxidized state following a final electron transfer from Fe^{II} to a second molecule of oxidized cyt *c*. The second IET step (from Mo^{V} to Fe^{III}) has been studied after photochemical reduction of the heme by one electron to the $Mo^{VI}Fe^{II}$ species (*20*−*25*). The rate constant of electron transfer to the Mo center (k_{ET}) can then be determined by monitoring the heme reoxidation (Figure 2, IET #2 in reverse) at 555 nm (*20*−*25*).

In light of the rapid IET rate constants (k_{ET} > 1000 s^{-1}) observed in this enzyme (*21*), one surprising finding from

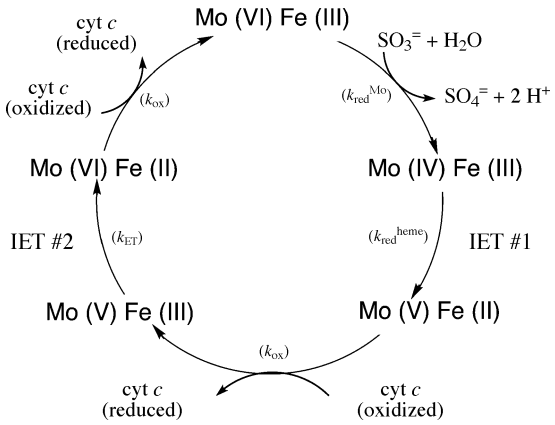

FIGURE 2: Reaction cycle of mammalian SO with oxidation-state changes indicated in the molybdenum (Mo) and heme (Fe) centers of the enzyme. The two intramolecular electron transfer (IET) steps where electrons are transferred from the Mo center to the heme center are shown. IET #1 occurs during the reductive half of the reaction cycle, while IET #2 occurs in the oxidative half of the reaction cycle as indicated.

analysis of the SO crystal structure was the large intramolecular distance of 32 Å between the Mo and Fe centers (*11*). The most likely explanation for this apparent discrepancy is that during the reaction cycle the two domains adopt a conformation that brings the Mo and heme centers much closer to each other. Indeed, the rate constant for IET decreases with an increase in the viscosity of the solution, indicating that domain movement is essential for efficient electron transfer between the heme and Mo domains of SO (*23*, *24*). In addition, analysis of the one-electron reduced paramagnetic ($Mo^{V}Fe^{III}$) form of SO by electron−electron double resonance (ELDOR) spectroscopy detected a range of Mo−Fe distances in solution (*26*).

On the basis of the crystal structure of chicken SO, five conserved residues form a positively charged substrate-binding pocket at the Mo center of human SO: three arginines at positions 160, 212, and 472 along with Tyr 343 and Trp 227. The importance of Arg 160 has been demonstrated by the isolation of the R160Q variant from a patient with SO deficiency. Analysis of the purified variant revealed a 1000-fold decrease in the second-order rate constant compared to that of wild-type SO (*27*), as well as a significantly decreased k_{ET} (*25*). Recent studies of the Y343F variant using flash photolysis (*24*) and stopped-flow kinetics (*13*) have also demonstrated the importance of Tyr 343 both in substrate binding and in facilitating IET between the Mo and heme metal centers.

Loss of SO activity due to either a defect in one of the proteins in the synthesis pathway for the MPT cofactor (cofactor deficiency) (*28*−*30*) or a mutation in the SO gene itself (isolated SO deficiency) leads to severe birth defects and neurological problems that usually result in death at an early age (*31*). Numerous mutations have been identified in the structural gene for human SO from patients exhibiting isolated SO deficiency (*11*, *27*, *32*−*35*). While some of these, such as R160Q (*25*, *27*) and C207S (*36*−*38*), have already been thoroughly characterized, for many of the identified substitutions, correlating loss of function in SO-deficient patients with alterations in the physical and biochemical properties of the variant enzyme has not yet been accomplished, due in part to the difficulty in obtaining a crystal structure for human SO. However, a very recent advance in which recombinant wild-type chicken SO and the R138Q (equivalent to human R160Q) variant were crystallized and structurally analyzed will allow more structure−function studies to be performed on SO variants (*39*).

The identification and initial characterization of mutations in human patients that cause destabilization of the dimer, including G473D, S370Y, and R211Q, suggested that oligomerization was critical for SO activity in vivo (*11*, *32*). Preliminary activity assays of these variants revealed in all cases a significant decrease in substrate binding ability and in catalytic efficiency.[2] On the basis of the crystal structure, it was hypothesized that the severe SO deficiency seen in a patient with the G473D mutation was the result of several factors (*11*). First, Gly 473 is located in a tight loop with torsion angles ($\phi = 62°$, $\varphi = 32°$) that are impossible for any other residue to adopt (Figure 1B). It should be noted that a Gly residue in this position is strictly conserved in all SO proteins isolated to date, including plant SO (*3*) and bacterial SDH (*5*). Second, the Gly 473 residue is buried deep within the dimerization domain of SO, and substitution of an Asp would place a charged residue near the residues Met 215 and Val 221, both of which form the hydrophobic face of an α-helix from the Mo domain that is inserted into the dimerization domain (Figure 1B). Finally, an Asp in that position would be expected to be in steric conflict with Arg 212, a residue critical for maintaining the positively charged substrate-binding pocket of SO (Figure 1B,C). In addition, any disruptions in folding severe enough to prevent dimerization could also be expected to impair the ability of SO to adopt the conformation necessary for efficient electron transfer between the Mo and heme domains of each subunit during the reaction cycle. The studies described here were designed to extend our understanding of the overall catalytic mechanism of this essential protein and the importance of oligomerization through detailed kinetic analyses of dimer-destabilized variants of human SO. To that end, the G473D patient variant of SO was analyzed for both oligomerization status and activity during steady-state and stopped-flow kinetic studies. The G473W variant was created to study SO in the monomeric state in the absence of the negative charge contributed by Asp. The G473A variant was created to test the effect of forcing a change in the torsion angles without the complication of the bulky charged Asp residue at that position. Finally, the double mutant R212A/G473D was created to relieve steric interference between Asp 473 and Arg 212.

MATERIALS AND METHODS

Site-Directed Mutagenesis of SO. DNA containing the SO gene with a G473D mutation was isolated from the cDNA of a human patient with SO deficiency and cloned into the pRG118 vector as previously described (*11*, *27*). We then introduced the patient-derived mutation into the pTG918 expression vector for wild-type human SO (*10*) by subcloning a fragment of the gene that contained the mutation from the pRG118 vector. The G473A, G473W, and R212A/G473D mutations were directly introduced into pTG918 (*10*) using the Transformer site-directed mutagenesis kit (Clontech). All constructs were verified by sequence analysis performed at the Duke University DNA Analysis Facility.

Expression and Purification of SO. All recombinant forms of SO were expressed in the TP1000 strain of *E. coli* and purified as previously described (*10*, *24*) with the following modifications. After the phenyl-Sepharose column, fractions exhibiting an A_{414}/A_{280} ratio of ≥ 0.90 were further purified using a Superdex 200 16/60 FPLC column (Amersham Pharmacia) equilibrated with 50 mM potassium phosphate buffer containing 0.1 mM EDTA at pH 7.80. Fractions exhibiting an A_{414}/A_{280} ratio of ≥ 0.98 were then pooled and used in the experiments described in this study. For gel filtration analysis of the oligomeric state of SO variants, purified protein (at 1 mg/mL) was injected onto a Zorbax GF 250 HPLC column equilibrated with 50 mM potassium phosphate buffer and eluted using a flow rate of 1 mL/min. The HPLC system consisted of a Hewlett-Packard 1090 solvent delivery system, and absorbance was monitored at 413 and 280 nm using an Agilent 1100 series photodiode array detector. The concentration of purified SO was determined from the A_{414} using an extinction coefficient of

[2] Graf, T. N. (2000) M.S. Thesis, Duke University, Durham, NC.

113 mM^{-1} cm^{-1}. The Mo content of the purified SO proteins was determined using a Varian SpectrAA-220 double-beam atomic absorption spectrometer, with sample preparation as previously described (*36*).

Steady-State Kinetics of SO. Steady-state kinetic assays were performed aerobically at 25 °C using a 1.0 cm path length cuvette in a Shimadzu UV-1601PC spectrophotometer. Assays were carried out in 20 mM buffers adjusted to the desired pH with acetic acid to minimize anion inhibition of SO as previously described (*13*, *19*). The buffers used were as follows: Bis-Tris at pH 6.0−6.5, Bis-Tris propane at pH 6.75−7.5, Tris at pH 7.5−8.75, and glycine at pH 8.75−10.0. The glycine buffers were adjusted to the desired pH using NaOH. Steady-state pH profiles were obtained using 15−50 μM horse heart cyt *c* (Sigma), 0.50−2.5 μg/mL SO, and varying concentrations of sulfite in a final assay volume of 1 mL. Assays used to determine $K_m^{cyt\ c}$ were performed at each pH value by holding the concentration of sulfite constant at $5K_m^{sulfite}$ and varying the concentration of cyt *c*. The reduction of cyt *c* was monitored at 550 nm using an extinction coefficient of 19 mM^{-1} cm^{-1}. The steady-state reaction parameters k_{cat} and K_m were obtained by a direct fit of the concentration dependence to the Michaelis−Menten equation. Steady-state assays with ferricyanide as the electron acceptor were performed using 20 mM buffers as described above, 40 μM ferricyanide, 1.5−5.0 μg/mL SO, and varying concentrations of sulfite in a final assay volume of 1 mL. The reduction of ferricyanide was monitored at 420 nm, and enzyme activity was reported in units per milligram, where 1 unit is equal to an absorbance change of 1.0 AU/min at 420 nm.

Stopped-Flow Assays of SO. Rapid reaction kinetic studies were performed using an SX.18MV stopped-flow reaction analyser (Applied Photophysics Ltd.) as previously described (*13*, *19*). The dead time of the instrument was determined to be <1.5 ms with a path length of 10 mm. To prepare the instrument for anaerobic operation, the sample tubing and valve lines were incubated with 250 mM sodium dithionite for several hours and then thoroughly rinsed with O_2-free water. Additionally, the sample-handling unit of the stopped-flow apparatus was fitted with an anaerobic accessory that enclosed the drive syringe plungers and was continuously flushed with nitrogen gas. The reaction temperature was maintained at 25 °C using a circulating water bath connected to the thermostat bath housing the drive syringes. All solutions were made anaerobic by being bubbled with argon gas for at least 30 min prior to use, and solutions of human SO were prepared by diluting <100 μL of a concentrated stock of the enzyme into a final volume of ~5 mL of anaerobic buffer. All dilutions were performed in an anaerobic chamber (Coy Laboratory Products Inc.), and 5 mL Hamilton gastight syringes were used to load samples into the stopped-flow spectrophotometer. Rapid kinetic assays of the reductive half-reaction were performed anaerobically at 25 °C using 0.3−0.8 μM protein. Reduction of the SO b_5-type heme was directly monitored by measuring the extinction change of the Soret peak at 425 or 430 nm. The k_{obs} of each reaction was obtained by fitting individual kinetic traces to single- or double-exponential curves using a nonlinear least-squares Levenberg−Marquardt algorithm. The maximal rate parameter k_{red} and the $K_d^{sulfite}$ for the reductive half-reactions were obtained by fitting the k_{obs} at varying sulfite concentrations to a hyperbolic curve as shown below.

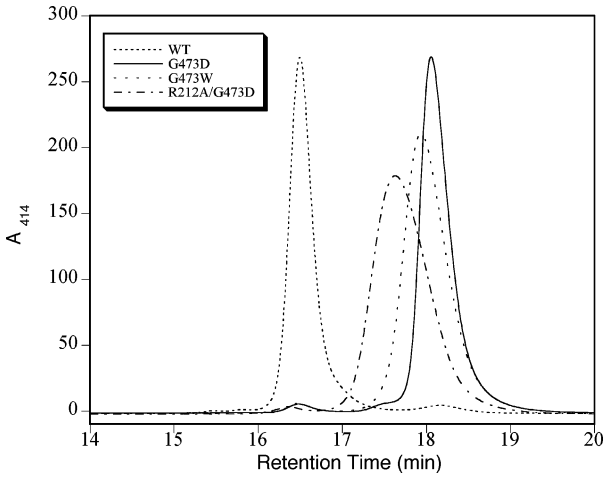

FIGURE 3: Gel filtration analysis of wild-type, G473D, G473W, and R212A/G473D SO. All proteins were injected at a concentration of 1 mg/mL and analyzed on a Zorbax GF-250 column as described in Materials and Methods.

$$k_{obs} = k_{red}[S]/(K_d + [S]) \quad (2)$$

Circular Dichroism. Circular dichroism (CD) spectra of both wild-type and variant human SO proteins were obtained using an Aviv 202 CD spectrometer. All samples contained 0.5−1.0 μM SO in 20 mM potassium phosphate (pH 7.60). CD spectral data were collected from 280 to 195 nm in 1 nm increments with 15−30 s averaging at each wavelength. The samples were maintained at 25 °C throughout data collection, and all data were collected at a dynode voltage below 500 V. After correction for the buffer signal, raw CD signals were converted to mean residue ellipticity ([θ]) expressed in degrees square centimeter per decimole.

Sedimentation Equilibrium Centrifugation. Sedimentation equilibrium analyses of wild-type and variant proteins were performed on a Beckman XLA analytical ultracentrifuge in 50 mM potassium phosphate and 0.5 mM EDTA (pH 7.8). In each case, three different concentrations of the protein (0.25, 0.50, and 1.0 mg/mL) were centrifuged to equilibrium first at 8000 rpm and then at 12 000 rpm at 4 °C. Scans were taken at 427 nm. Initial analysis and best-fit molecular masses were determined by the XLA-Ideal 1 software provided by Beckman using a calculated partial specific volume of 0.731 for all proteins. The monomer−dimer equilibrium molar concentrations were calculated using an appropriate ϵ_{427}, and the data were analyzed by a nonlinear universal fit of all data sets using a program kindly provided by A. Minton at the National Institutes of Diabetes and Digestive and Kidney Diseases (National Institutes of Health, Bethesda, MD).

RESULTS

The G473D variant of human SO was produced in recombinant *E. coli* and purified as described in Materials and Methods. Gel filtration (Figure 3) and sedimentation equilibrium experiments (Table 1) verified that the G473D variant exists primarily as a monomer, with a best-fit molecular mass of 54 kDa compared to the calculated mass of 52 kDa based on the amino acid sequence. In contrast,

Table 1: Sedimentation Equilibrium Parameters for Wild-Type, G473D, G473W, and R212A/G473D Human SO

	best-fit molecular mass[a] (kDa)	K_d (dimer/monomer)
wild type	101	2×10^{-7}
G473D	53.5	—[b]
G473W	54.5	—[b]
R212A/G473D	66.6	1×10^{-4}

[a] Three concentrations of each protein (0.25, 0.5, and 1.0 mg/mL) were centrifuged to equilibrium in 50 mM potassium phosphate and 0.5 mM EDTA (pH 7.8) at 4 °C as described in Materials and Methods. [b] No appreciable association observed.

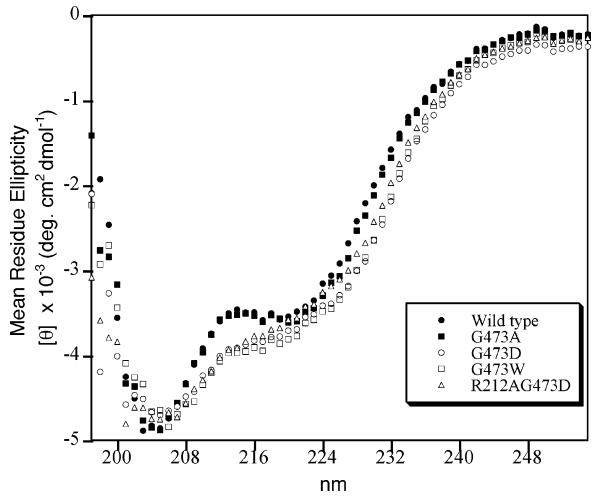

FIGURE 4: CD spectra of wild-type, G473A, G473D, G473W, and R212A/G473D human SO. CD spectral data were collected from 280 to 195 nm with protein samples at a concentration of 0.5−1.0 μM as described in Materials and Methods.

the best-fit molecular mass of the dimeric wild-type SO protein by sedimentation equilibrium analysis is 104 kDa (Table 1).

To explore the global effect of the G473D mutation on the folding of SO, this variant was also subjected to circular dichroism (CD) spectroscopy, a technique that can be used to estimate the secondary structure of a protein, to monitor changes in protein conformation upon environmental perturbations, or to compare the structure of a variant to that of the wild-type protein. As demonstrated in Figure 4, the CD spectrum of G473D was significantly altered from that of the wild-type protein. While the wild-type protein displayed typical mixed $\alpha + \beta$ secondary structure with a peak at 210 nm and a valley at 220 nm, G473D (with a loss of these characteristic structural features) exhibited a spectrum consistent with increased random coil secondary structure content (*40*). Atomic absorption (AA) analysis of the G473D mutant indicated incorporation of 0.92 mol of Mo/mol of protein, demonstrating that the secondary structure perturbations observed in this variant did not prevent Mo cofactor insertion.

Kinetic Assays of the G473D SO Variant. Steady-state assays were performed on G473D over the pH range 6−10 using cyt *c* as the terminal electron acceptor. Activity was severely impaired at all pH values and was particularly decreased at low pH (Table 2). The G473D variant also displayed a weakened ability to bind the substrate over the entire pH range, with $K_m^{sulfite}$ values ranging from 0.6 to 26 mM sulfite, which are several orders of magnitude higher than that of the wild-type protein. In contrast to assays performed on the wild-type protein, no activity could be detected above pH 9.5, even when very high concentrations of sulfite were used. The low k_{cat} combined with the high $K_m^{sulfite}$ resulted in specificity constants (k_{cat}/K_m) for G473D that were at least 5 orders of magnitude lower than those obtained for wild-type SO (Table 2).

Table 2: pH Dependence of Steady-State Kinetic Parameters for Human SO Variants

pH[a]	k_{cat} (s^{-1})	$K_m^{sulfite}$ (μM)	k_{cat}/K_m (M^{-1} s^{-1})
Wild Type[b]			
6.0	13.2 ± 0.4	1.29 ± 0.30	1.05×10^7
6.5	17.7 ± 0.3	1.62 ± 0.14	1.10×10^7
7.0	24.2 ± 0.3	2.72 ± 0.23	8.94×10^6
7.5	24.7 ± 0.4	3.39 ± 0.35	7.33×10^6
8.0	25.9 ± 0.2	4.35 ± 0.11	5.97×10^6
8.5	26.9 ± 0.5	8.25 ± 0.44	3.26×10^6
9.0	25.7 ± 0.9	22.1 ± 1.6	1.17×10^6
9.5	26.3 ± 1.5	67.1 ± 9.0	3.95×10^5
G473D			
6.0	0.14 ± 0.01	1660 ± 324	84.0
6.5	0.28 ± 0.01	990 ± 53	283
7.0	0.50 ± 0.02	623 ± 64	806
7.5	0.57 ± 0.01	1063 ± 18	538
8.0	0.58 ± 0.01	1223 ± 70	475
8.5	0.54 ± 0.03	2040 ± 30	265
9.1	0.42 ± 0.01	25878 ± 4825	16.2
9.6	UD[c]	—[d]	—[d]
G473A			
6.0	4.15 ± 0.50	4.53 ± 1.43	9.20×10^5
7.0	15.9 ± 0.1	5.36 ± 0.47	2.94×10^6
7.4	21.6 ± 0.7	17.2 ± 1.6	1.26×10^6
8.0	26.2 ± 0.4	48.7 ± 1.1	5.35×10^5
8.5	28.4 ± 1.2	107 ± 6	2.65×10^5
9.1	31.9 ± 0.3	774 ± 32	4.12×10^4
10.0	15.1 ± 1.5	3684 ± 504	4.10×10^3
G473W			
6.0	0.60 ± 0.02	1910 ± 238	314
7.0	1.80 ± 0.04	330 ± 41	5.46×10^3
8.5	2.48 ± 0.23	2034 ± 419	1.22×10^3
9.0	1.35 ± 0.37	10407 ± 4027	130
R212A/G473D			
7.0	UD[c]	—[d]	—[d]
8.5	UD[c]	—[d]	—[d]

[a] All buffers were at 20 mM and were titrated with acetic acid, except for glycine, which was at 50 mM and was titrated with NaOH. Assays were carried out at 25 °C as described in Materials and Methods. [b] Data adapted from ref *13*. [c] Undetectable activity. [d] Could not be determined in the absence of measurable activity.

The $K_m^{cyt\ c}$ for G473D was also determined at several pH values using saturating sulfite concentrations (at least 5 times greater than the $K_m^{sulfite}$ at each pH). At high pH, the $K_m^{cyt\ c}$ for G473D was comparable to the wild-type value (Table 3); however, at low pH, the G473D variant had a greatly weakened ability to interact with cyt *c* as demonstrated by a significant increase in $K_m^{cyt\ c}$ (Table 3 and Figure 5). Since the k_{cat} values for G473D in Table 2 were obtained using standard conditions that included a concentration of 50 μM cyt *c*, the lower k_{cat} values initially measured at pH 6.0 and 6.5 for G473D can be entirely attributed to an increase in the $K_m^{cyt\ c}$ at low pH. Accordingly, when higher concentrations of cyt *c* were used in the assays, the k_{cat} values increased significantly for pH 6.0 and 6.5 (Table 3), indicating that the k_{cat} for G473D changes very little from an average of ~0.5 s^{-1} over the entire range of pH values that was measured.

Ferricyanide is a nonspecific single-electron acceptor that (unlike cyt *c*) can directly interact with the Mo center of SO and is therefore not dependent on IET from the Mo center

Table 3: pH Dependence of $K_m^{cyt\ c}$ for Human SO Variants

pH[a]	k_{cat} (s^{-1})	$K_m^{cyt\ c}$ (μM)
Wild Type		
6.0	12.4	1.73
7.0	18.1	1.41
8.5	26.9	4.40
G473D		
6.0	0.34	107
6.5	0.53	63.5
7.0	0.78	36.2
7.5	0.62	14.0
8.0	0.59	4.74
8.6	0.48	3.71
G473A		
6.0	3.83	1.23
7.0	12.8	0.82
8.5	25.4	0.43
G473W		
6.0	1.67	90.5
7.0	2.94	35.7
8.5	1.95	5.36

[a] All buffers were at 20 mM were titrated with acetic acid. Assays were carried out at 25 °C as described in Materials and Methods.

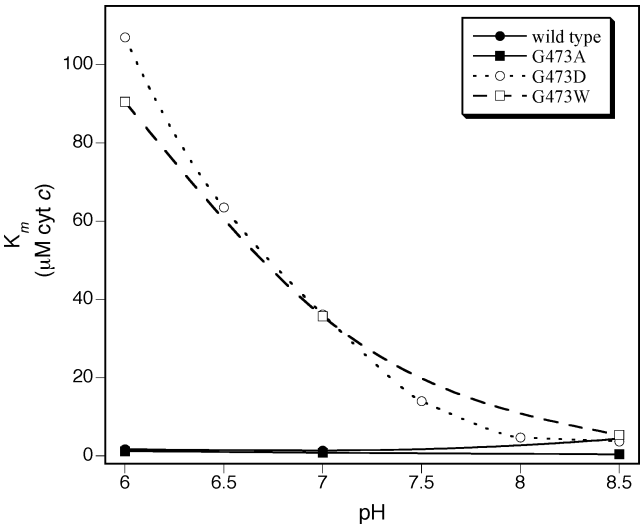

FIGURE 5: pH dependence of $K_m^{cyt\ c}$ for wild-type, G473A, G473D, and G473W human SO. Buffers were at 20 mM and were titrated with acetic acid. Assays were carried out at saturating sulfite concentrations (at least $5K_m^{sulfite}$) while varying the cyt *c* at 25 °C as described in Materials and Methods.

to the heme domain for reduction. When steady-state assays were performed using ferricyanide rather than cyt *c* as the terminal electron acceptor, the activity of G473D at pH 8.5 was ~10% of that of the wild type (Table 4); in contrast, the relative activity when cyt *c* was used as the electron acceptor was only ~2% of that of the wild-type protein at pH 8.5 (Tables 2 and 3). It should be noted that the $K_m^{sulfite}$ for G473D was higher in ferricyanide assays than when cyt *c* was used as the electron acceptor.

Using stopped-flow analysis, the reductive half-reaction (Figure 2, IET #1) of G473D was assessed by monitoring reduction of the heme from Fe^{III} to Fe^{II} at 425 nm. Like the results obtained in steady-state assays using ferricyanide as the terminal electron acceptor, the k_{red}^{heme} of G473D SO was approximately 10% of the wild-type value (8.73 and 83.3 s^{-1}, respectively, Table 5). At pH 8.5, the k_{red}^{heme} for wild-type human SO is approximately 3-fold higher than the

Table 4: Steady-State Kinetic Parameters Using Ferricyanide as the Electron Acceptor

pH[a]	V_{max} (units/mg)	$K_m^{sulfite}$ (μM)
Wild Type[b]		
7.0	78.0 ± 1.9	4.56 ± 0.27
8.6	99.8 ± 3.3	14.9 ± 0.8
G473D		
7.0	22.1 ± 1.0	26500 ± 1600
8.5	10.2 ± 0.76	41400 ± 7100
G473A		
7.0	29.8 ± 0.5	6.05 ± 0.46
8.5	67.8 ± 2.6	191 ± 4
G473W		
7.0	70.2 ± 2.8	21200 ± 900
8.5	28.8 ± 2.7	24000 ± 3600
R212A/G473D		
7.0	UD[c]	—[d]
8.5	UD[c]	—[d]

[a] Assays were carried out at 25 °C using 20 mM buffers, 40 μM ferricyanide, 0.5−10.0 μg/mL SO, and varying concentrations of sulfite as described in Materials and Methods. [b] Data adapted from ref *13*. [c] Undetectable activity. [d] Could not be determined in the absence of measurable activity.

Table 5: Reductive Half-Reaction Kinetic Parameters for Wild-Type and Variant SO Proteins

pH[a]	k_{red}^{heme} (s^{-1})	$K_d^{sulfite}$ (μM)	k_{red}/K_d ($M^{-1}\ s^{-1}$)
Wild Type[b]			
7.0	70.2	2.05	3.42×10^7
8.4	83.3	11.5	7.24×10^6
G473D			
8.5	8.73	5700	1.53×10^3
G473A			
7.0	180	71.4	2.52×10^6
8.5	226	700	3.23×10^5
G473W			
8.5	23.4	25300	924
R212A/G473D			
8.5	UD[c]	—[d]	—[d]

[a] All buffers were at 50 mM and were titrated with acetic acid. Assays were carried out anaerobically at 25 °C as described in Materials and Methods. [b] Data adapted from ref *13*. [c] Undetectable activity. [d] Could not be determined in the absence of measurable activity.

overall k_{cat} observed for the steady-state reaction (Table 5). The k_{red}^{heme} (8.73 s^{-1}) for G473D was also several-fold higher than the k_{cat} (0.5 s^{-1}) measured in steady-state assays.

Characterization of the G473A SO Variant. The G473D mutation was first identified in a patient with severe SO deficiency, and purification of the variant protein demonstrated that conversion of the small, uncharged Gly to the larger, charged Asp residue prevented dimerization of the protein. On the basis of analysis of the crystal structure of chicken SO (*11*), this was hypothesized to occur as a result of both steric and charge interference of the Asp 473 residue with the Arg 212, Met 215, and Val 221 residues (Figure 1). Additionally, Gly 473 is deeply buried in SO and exhibits torsion angles in the crystal structure not possible for any other residue to adopt. Thus, substitution of any residue at this position would be expected to have an effect on at least the local folding of the protein.

To further understand the importance of the Gly 473 torsion angles, the G473A variant was created using site-

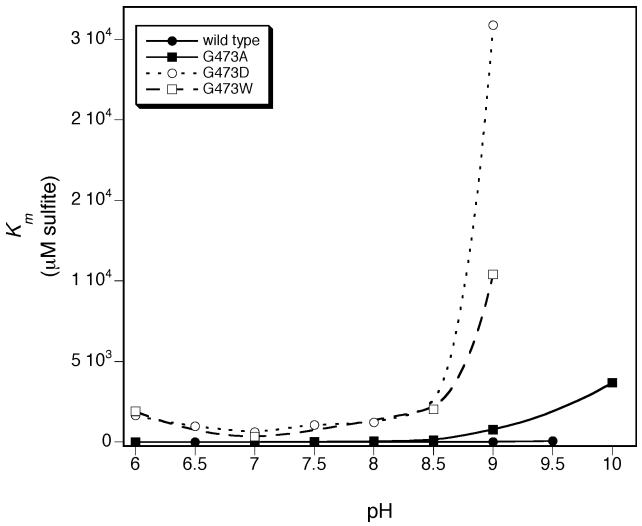

FIGURE 6: pH dependence of $K_m^{sulfite}$ for wild-type, G473A, G473D, and G473W human SO. Buffers were at 20 mM and were titrated with acetic acid, except for glycine, which was at 50 mM and was titrated with NaOH. Assays were carried out at 50 μM cyt *c* while varying the sulfite at 25 °C as described in Materials and Methods.

directed mutagenesis, produced recombinantly, and purified. AA analysis indicated that the purified protein had a nearly full complement of cofactor (0.91 mol of Mo/mol of protein). On the basis of gel filtration analysis (data not shown), replacement of glycine with alanine does not disrupt dimer formation, and in contrast to that of G473D, the CD spectrum of G473A is very similar to that of wild-type SO (Figure 4). While steady-state kinetic analysis demonstrated that the G473A protein has activity nearly identical to that of the wild-type protein at pH 8.5 (k_{cat} = 28.4 and 26.9 s^{-1}, respectively), the $K_m^{sulfite}$ of 107 μM at pH 8.5 is higher than the wild-type $K_m^{sulfite}$ of 8.3 μM (Table 2). Additionally, the G473A $K_m^{sulfite}$ increased significantly compared to that of wild-type SO above pH 8.0 (Table 2 and Figure 6), indicating that G473A has a greatly decreased ability to bind sulfite at high pH. The activity of G473A is also more sensitive to low pH, as demonstrated by a decrease in the k_{cat} at pH $\leq$7.0 (Tables 2 and 3).

In light of the impaired interaction of G473D with the electron acceptor cyt *c*, steady-state assays were performed on the G473A variant under saturating sulfite conditions (at least $5K_m^{sulfite}$) at pH 6.0, 7.0, and 8.5 with varying concentrations of cyt *c*. In contrast to that of the G473D variant, the $K_m^{cyt\ c}$ of G473A did not increase significantly at low pH, and G473A actually demonstrated a $K_m^{cyt\ c}$ slightly lower than that of the wild type at the pH values measured (Table 3). In steady-state assays using ferricyanide as the terminal electron acceptor, the G473A protein had slightly lower activity than the wild-type protein at pH 8.5 but was significantly impaired at pH 7.0 (Table 4), which is similar to the results observed in steady-state assays when cyt *c* was the terminal electron acceptor (Table 2).

Surprisingly, when stopped-flow rapid kinetics of the reductive half-reaction were performed on G473A SO, the k_{red}^{heme} for this protein was nearly 3 times the wild-type value at both pH 8.5 and 7.0 (Table 5). The $K_d^{sulfite}$ was also higher than that of the wild type, demonstrating a weakened ability to bind sulfite in this variant, consistent with results obtained in steady-state assays using either cyt *c* or ferricyanide as the terminal electron acceptor (Tables 2 and 4). The high $K_d^{sulfite}$ resulted in a second-order rate constant ($k_{red}/K_d^{sulfite}$) for G473A lower than that of the wild-type protein despite the high k_{red} values observed in this variant (Table 5).

Characterization of the G473W SO Variant. To further explore the importance of the Gly 473 residue in dimer formation, the G473W variant was created to replace Gly 473 with a large uncharged residue. This substitution was predicted to disrupt the dimer without the complicating factor of the negative charge contributed by the acidic Asp residue. During gel filtration purification of a very concentrated sample (>20 mg/mL) of this variant on a Superdex 200 16/60 column, the protein eluted as a broad peak midway between the retention times expected for a monomer and a dimer, indicating a rapid equilibrium between monomeric and dimeric forms (data not shown). However, when a more dilute sample (1 mg/mL) of the purified protein was similarly analyzed, the elution time was consistent with a monomeric state, albeit with a peak slightly broader than that of G473D (Figure 3). When the G473W variant was analyzed using sedimentation equilibrium centrifugation at 0.25−1.0 mg/mL, the protein showed no ability to associate into a dimer, with a best-fit molecular mass of 54.5 kDa, indicating that the protein exists primarily as a monomer at low protein concentrations (Table 1). When the secondary structure of this protein was analyzed using CD spectroscopy, the spectrum was very similar to that of G473D (Figure 4), indicating similar misfolding at the secondary structure level. As observed for the G473D variant, this misfolding had no effect on Mo cofactor binding with AA analysis indicating 0.90 mol of Mo/mol of protein.

When steady-state kinetic assays using cyt *c* as the terminal electron acceptor were performed from pH 6.0 to 9.0, G473W exhibited significantly (4−5-fold) higher activity than G473D; however, activity was still impaired relative to that of the wild-type protein (Table 2). In addition, the $K_m^{sulfite}$ of G473W was very similar to that of G473D, demonstrating that changing the Gly to a large bulky residue, regardless of charge, affects the ability of the active site to attract and bind sulfite (Table 2 and Figure 6). Like the results obtained with G473D, the G473W variant also demonstrated a significantly weakened ability to interact with the terminal electron acceptor cyt *c* at low pH values (Table 3 and Figure 5). In contrast, when ferricyanide was used as the terminal electron acceptor, the G473W variant demonstrated activity much higher than that observed for the G473D variant, and at pH 7.0, the activity was comparable to the wild-type value. However, the $K_m^{sulfite}$ remained very high, similar to the results obtained for G473D (Table 4).

When the reductive half-reaction of G473W was assessed using stopped-flow analysis, the protein did not behave with typical single-exponential kinetics, and fitting the kinetic traces to double-exponential traces revealed that there were two distinct rates. The first rate was approximately 30% as fast as the wild-type rate (k_{red} = 23.4 s^{-1}, Table 5), while the second was much slower with a k_{red} of <1 s^{-1} (data not shown). In addition, the $K_d^{sulfite}$ was extremely high, even compared to that of G473D. Since the first rate represented only a fraction of the overall amplitude of the reductive trace, it appears that only a small portion of the G473W protein had the ability to efficiently reduce the heme in the first IET of the reaction cycle.

Characterization of the R212A/G473D Variant. Mapping of the G473D mutation onto the chicken SO crystal structure predicts that the Asp 473 residue will be in steric conflict with Arg 212, preventing the C-terminal domain from folding to the native structure and precluding dimerization (*11*). In an attempt to relieve the steric conflict of Asp 473 with Arg 212, the double mutant R212A/G473D was generated and purified. When this variant was analyzed using size exclusion gel filtration chromatography on a dilute purified sample, the protein eluted in a broad peak midway between the elution expected for a monomer and a dimer, indicating an equilibrium between monomeric and dimeric forms (Figure 3). When R212A/G473D was analyzed using sedimentation equilibrium centrifugation, the protein had a best-fit molecular mass of 66.6 kDa and a K_d of 1×10^{-4}, indicating an improved ability to associate into a dimer compared to the abilities of both G473D and G473W (Table 1). AA analysis verified that this variant retained the ability to bind the Mo cofactor with 0.81 mol of Mo/mol of protein. When the secondary structure of R212A/G473D was analyzed using CD spectroscopy, its spectrum was very similar to those of both G473D and G473W (Figure 4), indicating that the overall secondary structure fold in each of these three variants is similar, despite their varying abilities to oligomerize. In steady-state kinetic assays of R212A/G473D using either cyt *c* or ferricyanide as the electron acceptor, the protein exhibited no detectable activity. In addition, stopped-flow analysis revealed that the protein was extremely resistant to reduction, even at very high sulfite concentrations. Therefore, despite the improved ability of the R212A/G473D double variant to dimerize compared to either G473D or G473W, the protein was completely inactive and was not further analyzed.

DISCUSSION

Activity measurements on recombinant G473D human SO showed a severe attenuation of catalytic activity as expected from the pathological sequalae of the mutation. Gel filtration and sedimentation equilibrium analyses revealed the monomeric nature of this variant, and detailed kinetic analysis indicated a much higher K_m for both sulfite and cyt *c*. While the exact concentration of sulfite in mitochondria is not known, it is expected to fluctuate due to dietary and environmental factors. A recent study in which intact rat brain mitochondria were exposed to micromolar levels of sulfite demonstrated severe inhibition of ATP production and glutamate dehydrogenase activity in a dose-dependent manner from 25 to 100 μM sulfite (*41*). Clearly, a variant with a high K_m for sulfite such as G473D would be essentially inactive in vivo until sulfite had already reached toxic, cell-damaging levels. To pinpoint the precise cause of the catastrophic consequences of this mutation on the structural and functional properties of the enzyme, we undertook detailed studies of the effects of several substitutions at Gly 473 using steady-state and rapid reaction kinetics to examine the catalytic parameters and physicochemical and spectroscopic probes to study perturbations in structural properties.

On the basis of the crystal structure of chicken SO, several possibilities for explaining the severe effect of the G473D mutation on the structure and activity of the enzyme existed (*11*). The Gly 473 residue is buried deeply in the dimerization interface of the Mo domain of SO. In all, some 30 electrostatic interactions, including salt bridges and H-bonds, constitute the dimerization interface between the two subunits. The insertion of an acidic residue such as Asp could alter the folding pathway of the domain to cause a redistribution of the charges in a manner that would result in fewer charge and surface interactions between the subunits, thus disrupting dimerization. The fact that the Mo-binding and heme domains of all the variants in this study contained full complements of their respective cofactors indicates that the perturbations in the secondary structure revealed by the CD spectra were most likely due to changes in the C-terminal dimerization domain, rather than global misfolding of the enzyme.

Gly 473 is also near several residues that are important for the formation of the substrate-binding pocket and active site. The change to a negatively charged residue would be expected to disrupt sulfite binding due to steric and charge effects on the residues Arg 212 and Arg 472, both of which are essential for maintaining the positive charge of the substrate-binding pocket (Figure 1C). Furthermore, Gly 473 is located in a very tight loop (Figure 1B), and the torsion angles exhibited by Gly 473 in the crystal structure are impossible for any other residue to adopt. Substitution of an Asp in that position would be expected to create steric and charge interference with the hydrophobic residues Met 215 and Val 221, which constitute the hydrophobic face of a short α-helix that is inserted deeply within the dimerization domain (Figure 1B).

Steady-state assays using cyt *c* as the terminal electron acceptor demonstrated that the G473D protein is severely inhibited in substrate binding and in overall catalysis (Table 2). G473D exhibited less impairment of activity when ferricyanide was used as the terminal electron acceptor rather than cyt *c*, and the rate constant of the reductive half-reaction (k_{red}^{heme}) was also low, indicating that changing Gly to the charged residue Asp inhibits the first IET step from Mo to heme but that the transfer of electrons to ferricyanide and, by inference, the oxidation of sulfite at the Mo center are much less affected. While significantly lower than the wild-type k_{red}^{heme} of 83.3 s^{-1}, the rate constant for the reductive half-reaction ($k_{red}^{heme} = 8.73$ s^{-1}) was still much higher than the overall k_{cat} (0.54 s^{-1}) at pH 8.5, indicating that other factors in addition to the attenuated rate of the first IET contribute to the low activity of the G473D variant. In support of these observations, recent data using flash photolysis indicate significant impairment in the second IET in G473D, leading to the conclusion that this is the rate-limiting step in G473D SO (*42*).

Analysis of the G473W Variant. Sedimentation equilibrium and CD analyses performed on the G473W variant demonstrated that substitution of a bulky residue for Gly 473, regardless of charge, deleteriously affects folding at the secondary structure level. Gel filtration (Figure 3) and sedimentation equilibrium (Table 1) experiments demonstrated that G473W exists primarily as a monomer at low protein concentrations. CD analysis indicated that this variant also had secondary structure perturbations and an increased level of random coil formation, with a spectrum very similar to that of G473D (Figure 4). While demonstrating a somewhat higher catalytic efficiency than G473D, G473W remained impaired compared to the wild-type protein, despite the absence of the negative charge contributed by Asp in

G473D. The steady-state kinetic results for G473W indicated an activity approximately 5-fold higher than that of G473D; however, the $K_m^{sulfite}$ was quite similar to that of G473D, indicating that the size of the residue at this position, regardless of charge, significantly affects substrate binding (Table 1).

The fact that G743D and G473W had similar $K_m^{sulfite}$ values indicates that the negative charge of an Asp residue at this position does not directly affect the positive charge of the substrate-binding pocket; rather, there is most likely a steric effect on the residues which do form the substrate-binding pocket in both of these variants. In the absence of the crystal structure of these variants, it cannot be stated definitively which neighboring residues are affected by these mutations. However, in the wild-type chicken SO crystals, Gly 473 is quite close to several residues that are essential for maintaining the positively charged substrate-binding pocket, including Arg 160, Arg 212, and Arg 472 (Figure 1C). In addition, the $K_m^{sulfite}$ increased significantly at high pH (Figure 6) in both G473D and G473W. An increase in $K_m^{sulfite}$ at high pH also occurs in the wild-type protein (Table 2). On the basis of previous studies of chicken SO (*19*) and wild-type and Y343F human SO (*13*), this increase has been proposed to be due to deprotonation of the Tyr 322 residue (Tyr 343 in human) in the active site. It is clear that this effect is much more significant in both G473W and G473D, with an exponential increase in the $K_m^{sulfite}$ above pH 9 (Figure 6). The $K_m^{sulfite}$ was lowest in both G473W and G473D at pH 7.0 but then increased again below that pH, possibly due to protonation of another residue in the active site or even to protonation of the sulfite substrate itself ($pK_a \sim 7$ for HSO_3^-/SO_3^{2-}). The wild-type enzyme is able to oxidize bisulfite efficiently (*19*) and possibly even preferentially (*13*), but it is possible that changes in the active site of these variants result in a preference for the deprotonated form of the substrate.

Steady-state assays using ferricyanide as the electron acceptor showed significantly higher activity for G473W than for G473D, particularly at pH 7.0, where G473W had nearly wild-type activity, though the $K_m^{sulfite}$ remained very high. This result reinforces the importance of a proper interaction between the Mo and heme domains for effective IET during the reaction cycle (*23*, *24*), since this is not necessary when ferricyanide rather than cyt *c* is used as the electron acceptor. In agreement with these results, recent flash photolysis assays have directly measured a very low rate constant when observing the reverse IET in G473W (*42*), indicating that this is the rate-limiting step in the overall reaction for this variant.

Stopped-flow analysis of the G473W reductive half-reaction identified two rates: a rapid rate representing only a very small fraction of the overall amplitude of the reductive trace at 425 nm and a much slower rate representing the majority of the overall amplitude. On the basis of the sedimentation equilibrium results for G473W, it is likely that the majority of the protein was in a monomeric state at the concentration at which stopped-flow reactions were performed. It is possible that the initial rapid rate represents the minor fraction of the enzyme in a dimeric state, while the slower rate represents the monomeric fraction of the protein.

A particularly interesting aspect of the G473D and G473W variants was the significant increase in $K_m^{cyt\ c}$ at low pH (Table 3 and Figure 5). It was somewhat surprising that the ability to interact with cyt *c* was affected in both G473D and G473W, since Gly 473 is far removed from the N-terminal heme domain in the crystal structure of chicken SO. Furthermore, the Mo and heme domains fold independently of each other when synthesized separately, are attached by only a flexible loop, and presumably can have different orientations with respect to each other. The results indicating the loss of ability to interact with cyt *c* in G473D and G473W at low pH provide evidence that interaction of the heme domain with the exogenous electron acceptor cyt *c* can be affected by misfolding in the Mo domain, even though the heme domain itself is properly folded and contains a full complement of the heme cofactor. Previous studies showed that in reduced SO, the heme domain swivels around the hinge for optimal contact with the Mo domain to allow efficient IET (*23*, *24*). The results of this study provide evidence that the heme domain may also need to specifically interact or dock with the Mo domain to allow productive contact with cyt *c* since this interaction is clearly impaired in both G473D and G473W. The SO protein may adopt two (or more) different Mo−heme domain interactions during the reaction cycle: one conformation would allow for productive IET, while a second interaction would facilitate productive electron transfer between the heme domain and cyt *c*. The fact that this interaction is impaired at only low pH in G473W and G473D indicates that the heme domain likely interacts in an electrostatic manner with residues in the Mo domain, and enough rearrangement has occurred in these variants to disrupt this interaction upon protonation of these residues at low pH.

The concentration of cyt *c* in the mitochondria has been estimated to be 400 μM (*43*, *44*); however, as it is loosely associated with the intermembrane, the concentration likely varies widely even within the mitochondrial space. Cyt *c* is involved in many processes, including those in the electron transfer chain and in oxidative radical scrubbing, and even a moderately higher $K_m^{cyt\ c}$ such as that observed in G473D and G473W could adversely affect the ability of the mitochondria to remove the toxic sulfite metabolite.

Analysis of the G473A Variant. Although the torsion angles adopted by glycine in the native crystal structure ($\phi = 62°$, $\varphi = 32°$) are impossible for alanine to adopt (*11*), the G473A variant was dimeric and had a CD spectrum comparable to that of the wild type (Figure 4), indicating that substitution of an alanine for the glycine at position 473 has little effect on the overall secondary structure of the protein and that only localized structural changes occur to accommodate this substitution. The lack of an increase in $K_m^{cyt\ c}$ at low pH for G473A (Table 3 and Figure 5) further indicated that only local perturbations were caused by the introduction of an alanine and that these did not disrupt interaction of the heme domain with cyt *c*. The steady-state activity of G473A was nearly identical to that of the wild type at pH $\geq$7.5, though the protein was less active at low pH (Table 1). Moreover, the $K_m^{sulfite}$ was significantly higher than that of the wild type, indicating that even a small increase in the size of the side chain at that position, regardless of charge, interferes with the ability of the active site pocket to attract and bind sulfite, particularly at high pH (Table 1 and Figure 6). While this

effect is less pronounced in G473A than in either G473D or G473W, the residues in the active site most likely directly affected by the substitution of an Ala are Arg 212 and Arg 472 (Figure 1C). Both high $K_m^{sulfite}$ and sensitivity to low pH were also observed in steady-state assays using ferricyanide as the terminal electron acceptor.

Especially interesting are stopped-flow results demonstrating a very rapid rate constant (~3-fold higher than the wild-type value) for the reductive half-reaction (k_{red}) of G473A at both pH 8.5 and 7.0. The $K_d^{sulfite}$ was also very high in stopped-flow assays. According to the model for the reaction cycle of SO (*13*), release of the product (sulfate) is necessary for the first IET to occur. A higher $K_d^{sulfite}$ as observed in G473A could facilitate release of the sulfate and more rapid IET. In contrast, studies of IET #2 in the G473A variant did not indicate an IET faster than that of the wild type (*42*), consistent with the fact that product release is not the limiting parameter for the second IET in the oxidative half of the reaction cycle. The direct neighbor of Gly 473 is Arg 472 (Figure 1C), a residue that has been proposed to be essential in IET between the Mo and heme domains, on the basis of a significant change in orientation of the Arg 472 (Arg 450 in chicken SO) side chain depending on the presence or absence of sulfate in the active site pocket (*39, 45*). It is possible that the insertion of the slightly larger Ala at this position affects the orientation of Arg 472 in a manner that results in a faster rate for the first IET in the reductive half-reaction. Despite the increase in k_{red}, the k_{cat} of G473A was quite similar to that of the wild type, indicating that the reductive half-reaction including the first IET is not rate-limiting in this variant.

Analysis of the R212A/G473D Variant. On the basis of the SO crystal structure (*11*), Asp 473 in G473D SO was proposed to be in steric conflict with Arg 212, a residue critical for maintaining the positively charged substrate-binding pocket of SO (Figure 1B,C). Therefore, the R212A/G473D variant was created to remove this steric conflict and possibly yield a dimeric variant of G473D. While the R212A/G473D variant did indeed regain some ability to dimerize compared to both G473D and G473W (Table 1), the protein was completely inactive, in both steady-state and stopped-flow assays. In agreement with these results, measurement of the IET using flash photolysis also yielded no measurable electron transfer in this mutant (*42*). The lack of activity of this protein, despite the partial recovery of dimerization ability (Table 1), can be explained in light of the deleterious effects of the individual G473D or R212A mutation. Preliminary results from kinetic analysis of the R212A variant indicate a greatly decreased k_{cat} (0.10 s^{-1}) and an increased $K_m^{sulfite}$ (570 μM) compared to those of wild-type SO, despite existing as a dimer and having a full complement of the Mo cofactor.[2] The combination of these deleterious mutations likely resulted in the complete loss of the ability to bind and oxidize sulfite. In addition, the CD spectrum of R212A/G473D was remarkably similar to those of both G473D and G473W, showing that while the double variant regained a partial ability to dimerize compared to the single variants, there was still significant misfolding at the secondary structure level (Figure 4).

Future studies utilizing SO variants in which dimerization has been prevented without severe perturbation of the protein backbone would help to further clarify the importance of the dimer in the activity of the protein. One possible candidate is the pathologic monomeric mutant R211Q. Preliminary gel filtration during purification of the R211Q variant revealed two distinct peaks corresponding to dimeric and monomeric forms, with the dimeric fraction having activity much higher than what has been observed for any other monomeric mutant.[2] This activity is rapidly lost upon dilution, making R211Q a promising candidate for future studies of the importance of dimerization in the activity of SO.

While all mammalian SO proteins isolated to date are dimeric, characterization of a bacterial member of the SO family (SDH from *Starkeya novella*) revealed that it exists as a heterodimeric complex consisting of a Moco-binding subunit and a heme-containing subunit, corresponding to a single subunit of mammalian SO (*5*). Furthermore, the two subunits most likely do not move relative to each other during IET or the rest of the reaction cycle, as suggested by the fact that viscosity and sulfate anions have no effect on the rate of IET between the Mo and heme centers (*46*). Recent elucidation of the structure of *S. novella* SDH revealed that the orientation of the heme subunit with respect to the molybdenum domain in the bacterial enzyme is quite different from that in chicken SO (*47*). The heme domain orientation in chicken SO could be modeled to resemble that of the bacterial enzyme without any steric conflict. Indeed, the near wild-type activity of G473W in the ferricyanide assay (Table 4) suggests that if the heme domain of mammalian SO had the same fixed orientation as seen in the bacterial protein, the IET of the mutant might also be normal.

Despite significant differences in the quaternary structure, the Cα trace of the Mo domain of bacterial SDH was very similar to that of chicken SO, with an rms deviation of only 1.34 (*47*). The fact that bacterial SDH does not dimerize, and that all of the monomeric variants of human SO in this study demonstrated significant backbone perturbation, indicates that monomerization may be a "symptom" rather than the underlying cause of the low activity and other impairment seen in these variants. Superposition of the structure of the chicken SO and bacterial SDH proteins revealed that a loop found in the dimerization domain adopts a significantly different conformation in these two proteins, with the bacterial SDH loop including a disulfide bond (between Cys 243 and Cys 245) that most likely precludes dimerization of that protein (*47*). Future study of the mammalian SO protein could include specific Cys substitutions in the dimerization domain designed to create a disulfide bond in the loop, possibly disrupting the salt bridges and H-bonds of the dimerization interface. These mutations would, we hope, have a limited peripheral effect on either the overall secondary structure of the protein or the substrate-binding pocket, allowing future studies to resolve the importance of dimerization in the activity of mammalian SO. In addition, the recent success in crystallization and structural analysis of recombinant chicken SO and the R138Q variant (analogous to R160Q in human SO) holds great promise for future structure−function studies of the G473D variant as well as other variants with impaired dimerization ability (*39*). These studies are currently in progress.

In conclusion, the data presented in this study directly demonstrate several specific causes for the significant

impairment of function that resulted in severe SO deficiency in the human patient with the G473D mutation. Characterization of the G473W variant demonstrated the deleterious effect of changing the glycine residue at that position to a larger residue, regardless of charge. The G473D and G473W variants both had weakened ability for productive interaction between the Mo and heme domains for effective electron transfer. The studies presented here have also demonstrated the importance of proper folding of the Mo domain for the heme domain to properly interact with cyt *c*, particularly at low pH. These results suggest that optimal interaction between the two domains is necessary not only for IET but also for the final electron transfer to cyt *c* from the heme domain of SO.

ACKNOWLEDGMENT

We thank Sandra Jaramillo-Busquets and Kayla Capps for technical assistance in protein purification and enzyme assays. We also thank Dr. Margot Wuebbens for helpful discussions, Dr. Terry G. Oas and members of his laboratory for help in use of the CD spectrophotometer, and Dr. Harvey Sage for performing the sedimentation equilibrium experiments. We gratefully acknowledge Drs. John Enemark, Gordon Tollin, and Changjian Feng of the University of Arizona (Tucson, AZ) for helpful discussions and critical reading of the manuscript.

REFERENCES

1. Schindelin, H., Kisker, C., and Rajagopalan, K. V. (2001) Molybdopterin from molybdenum and tungsten enzymes, *Adv. Protein Chem. 58*, 47−94.
2. Wuebbens, M. M., and Rajagopalan, K. V. (2003) Mechanistic and mutational studies of *Escherichia coli* molybdopterin synthase clarify the final step of molybdopterin biosynthesis, *J. Biol. Chem. 278*, 14523−14532.
3. Eilers, T., Schwarz, G., Brinkmann, H., Witt, C., Richter, T., Nieder, J., Koch, B., Hille, R., Hänsch, R., and Mendel, R. R. (2001) Identification and biochemical characterization of *Arabidopsis thaliana* sulfite oxidase. A new player in plant sulfur metabolism, *J. Biol. Chem. 276*, 46989−46994.
4. Campbell, W. H. (1999) Nitrate reductase structure, function and regulation: Bridging the gap between biochemistry and physiology, *Annu. Rev. Plant Physiol. 50*, 277−303.
5. Kappler, U., Bennett, B., Rethmeier, J., Schwarz, G., Deutzmann, R., McEwan, A. G., and Dahl, C. (2000) Sulfite:cytochrome *c* oxidoreductase from *Thiobacillus novellus*. Purification and molecular biology of a heterodimeric member of the sulfite oxidase family, *J. Biol. Chem. 275*, 13202−13212.
6. Rajagopalan, K. V., and Johnson, J. L. (2002) Sulfite Oxidase, in *Wiley Encyclopedia of Molecular Medicine* (Creighton, T. E., Ed.) pp 3048−3051, John Wiley and Sons, New York.
7. Enemark, J. H., and Cosper, M. M. (2002) Molybdenum Enzymes and Sulfur Metabolism, in *Metal Ions in Biological Systems* (Sigel, A., and Sigel, H., Eds.) Vol. 39, pp 621−654, Marcel Dekker, New York.
8. Garrett, R. M., and Rajagopalan, K. V. (1994) Molecular cloning of rat liver sulfite oxidase. Expression of a eukaryotic Mo-pterin-containing enzyme in *Escherichia coli*, *J. Biol. Chem. 269*, 272−276.
9. Garrett, R. M., Bellissimo, D. B., and Rajagopalan, K. V. (1995) Molecular cloning of human liver sulfite oxidase, *Biochim. Biophys. Acta 1262*, 147−149.
10. Temple, C. A., Graf, T. N., and Rajagopalan, K. V. (2000) Optimization of expression of human sulfite oxidase and its molybdenum domain, *Arch. Biochem. Biophys. 383*, 281−287.
11. Kisker, C., Schindelin, H., Pacheco, A., Wehbi, W. A., Garrett, R. M., Rajagopalan, K. V., Enemark, J. H., and Rees, D. C. (1997) Molecular basis of sulfite oxidase deficiency from the structure of sulfite oxidase, *Cell 91*, 973−983.
12. Johnson, J. L., and Rajagopalan, K. V. (1977) Tryptic cleavage of rat liver sulfite oxidase. Isolation and characterization of molybdenum and heme domains, *J. Biol. Chem. 252*, 2017−2025.
13. Wilson, H. L., and Rajagopalan, K. V. (2004) The role of tyrosine 343 in substrate binding and catalysis by human sulfite oxidase, *J. Biol. Chem. 279*, 15105−15113.
14. Astashkin, A. V., Raitsimring, A. M., Feng, C., Johnson, J. L., Rajagopalan, K. V., and Enemark, J. H. (2002) Pulsed EPR studies of nonexchangeable protons near the Mo(V) center of sulfite oxidase: Direct detection of the α-proton of the coordinated cysteinyl residue and structural implications for the active site, *J. Am. Chem. Soc. 124*, 6109−6118.
15. Astashkin, A. V., Raitsimring, A. M., Feng, C., Johnson, J. L., Rajagopalan, K. V., and Enemark, J. H. (2002) The Mo−OH proton of the low pH form of sulfite oxidase: Comparison of the hyperfine interactions obtained from pulsed ENDOR, CW-EPR and ESEEM measurements, *Appl. Magn. Reson. 22*, 421−430.
16. Astashkin, A. V., Feng, C., Raitsimring, A. M., and Enemark, J. H. (2005) ^{17}O ESEEM evidence for exchange of the axial oxo ligand in the molybdenum center of the high pH form of sulfite oxidase, *J. Am. Chem. Soc. 127*, 502−503.
17. Raitsimring, A. M., Pacheco, A., and Enemark, J. H. (1998) ESEEM investigations of the high pH and low pH forms of chicken liver sulfite oxidase, *J. Am. Chem. Soc. 120*, 11263−11278.
18. Brody, M. S., and Hille, R. (1995) The reaction of chicken liver sulfite oxidase with dimethylsulfite, *Biochim. Biophys. Acta 1253*, 133−135.
19. Brody, M. S., and Hille, R. (1999) The kinetic behavior of chicken liver sulfite oxidase, *Biochemistry 38*, 6668−6677.
20. Sullivan, E. P., Jr., Hazzard, J. T., Tollin, G., and Enemark, J. H. (1992) Inhibition of intramolecular electron transfer in sulfite oxidase by anion binding, *J. Am. Chem. Soc. 114*, 9662−9663.
21. Sullivan, E. P., Jr., Hazzard, J. T., Tollin, G., and Enemark, J. H. (1993) Electron transfer in sulfite oxidase: Effects of pH and anions on transient kinetics, *Biochemistry 32*, 12465−12470.
22. Pacheco, A., Hazzard, J. T., Tollin, G., and Enemark, J. H. (1999) The pH dependence of intramolecular electron transfer rates in sulfite oxidase at high and low anion concentrations, *J. Biol. Inorg. Chem. 4*, 390−401.
23. Feng, C., Kedia, R. V., Hazzard, J. T., Hurley, J. K., Tollin, G., and Enemark, J. H. (2002) Effect of solution viscosity on intramolecular electron transfer in sulfite oxidase, *Biochemistry 41*, 5816−5821.
24. Feng, C., Wilson, H. L., Hurley, J. K., Hazzard, J. T., Tollin, G., Rajagopalan, K. V., and Enemark, J. H. (2003) Role of conserved tyrosine 343 in intramolecular electron transfer in human sulfite oxidase, *J. Biol. Chem. 278*, 2913−2920.
25. Feng, C., Wilson, H. L., Hurley, J. K., Hazzard, J. T., Tollin, G., Rajagopalan, K. V., and Enemark, J. H. (2003) Essential role of conserved arginine 160 in intramolecular electron transfer in human sulfite oxidase, *Biochemistry 42*, 12235−12242.
26. Codd, R., Astashkin, A. V., Pacheco, A., Raitsimring, A. M., and Enemark, J. H. (2002) Pulsed ELDOR spectroscopy of the Mo(V)/Fe(III) state of sulfite oxidase prepared by one-electron reduction with Ti(III) citrate, *J. Biol. Inorg. Chem. 7*, 338−350.
27. Garrett, R. M., Johnson, J. L., Graf, T. N., Feigenbaum, A., and Rajagopalan, K. V. (1998) Human sulfite oxidase R160Q. Identification of the mutation in a sulfite oxidase deficient patient and expression and characterization of the mutant enzyme, *Proc. Natl. Acad. Sci. U.S.A. 95*, 6394−6398.
28. Johnson, J. L., Rajagopalan, K. V., and Wadman, S. K. (1993) Human molybdenum cofactor deficiency, *Adv. Exp. Med. Biol. 338*, 373−378.
29. Johnson, J. L., Wuebbens, M. M., Mandell, R., and Shih, V. E. (1988) Molybdenum cofactor deficiency in a patient previously characterized as deficient in sulfite oxidase, *Biochem. Med. Metab. Biol. 40*, 86−93.
30. Duran, M., de Bree, P. K., de Klerk, J. B. C., Dorland, L., and Berger, R. (1996) Molybdenum cofactor deficiency: Clinical presentation and laboratory diagnosis, *Int. Pediatr. 11*, 334−338.
31. Johnson, J. L., and Duran, M. (2001) Molybdenum Cofactor Deficiency and Isolated Sulfite Oxidase Deficiency, in *The Metabolic and Molecular Bases of Inherited Disease* (Scriver, C. R., et al., Eds.) 8th ed., pp 3163−3177, McGraw-Hill, New York.
32. Johnson, J. L., Coyne, K. E., Garrett, R. M., Zabot, M. T., Dorche, C., Kisker, C., and Rajagopalan, K. V. (2002) Isolated sulfite oxidase deficiency: Identification of 12 novel SUOX mutations in 10 patients, *Hum. Mutat. 20*, 74.

33. Johnson, J. L., Rajagopalan, K. V., Renier, W. O., Van der Burgt, I., and Ruitenbeek, W. (2002) Isolated sulfite oxidase deficiency: Mutation analysis and DNA-based prenatal diagnosis, *Prenatal Diagn. 22*, 433−436.
34. Lam, C., Li, C., Lai, C., Tong, S., Chan, K., Ng, G. S., Yuen, Y., Cheng, A. W., and Chan, Y. (2002) DNA-based diagnosis of isolated sulfite oxidase deficiency by denaturing high-performance liquid chromatography, *Mol. Genet. Metab. 75*, 91−95.
35. Lee, H. F., Mak, B. S. C., Chi, C. S., Tsai, C. R., Chen, C. H., and Shu, S. G. (2002) A novel mutation in neonatal isolated sulphite oxidase deficiency, *Neuropediatrics 33*, 174−179.
36. Garrett, R. M., and Rajagopalan, K. V. (1996) Site-directed mutagenesis of recombinant sulfite oxidase. Identification of cysteine 207 as a ligand of molybdenum, *J. Biol. Chem. 271*, 7387−7391.
37. George, G. N., Garrett, R. M., Prince, R. C., and Rajagopalan, K. V. (1996) The molybdenum site of sulfite oxidase: A comparison of the wild-type and the cysteine 207 to serine mutant using X-ray absorption spectroscopy, *J. Am. Chem. Soc. 118*, 8588−8592.
38. George, G. N., Garrett, R. M., Prince, R. C., and Rajagopalan, K. V. (2004) Coordination chemistry at the molybdenum site of sulfite oxidase: Redox-induced structural changes in the cysteine 207 to serine mutant, *Inorg. Chem. 43*, 8456−8460.
39. Karakas, E., Wilson, H. L., Graf, T. N., Xiang, S., Jaramillo-Busquets, S., Rajagopalan, K. V., and Kisker, C. (2005) Structural insights into sulfite oxidase deficiency, *J. Biol. Chem. 280*, 33506−33515.
40. Cantor, C. R., and Schimmel, P. R. (1980) *Techniques for the study of biological structure and function*, W. H. Freeman and Company, New York.
41. Zhang, X., Vincent, A. S., Halliwell, B., and Wong, K. P. (2004) A mechanism of sulfite neurotoxicity: Direct inhibition of glutamate dehydrogenase, *J. Biol. Chem. 279*, 43035−43045.
42. Feng, C., Wilson, H. L., Tollin, G., Astashkin, A. V., Hazzard, J. T., Rajagopalan, K. V., and Enemark, J. H. (2005) The pathogenic sulfite oxidase mutants G473D and A208D are defective in intramolecular electron transfer, *Biochemistry 44*, 13734−13743.
43. Radi, R., Turrens, J. F., and Freeman, B. A. (1991) Cytochrome *c*-catalyzed membrane lipid peroxidation by hydrogen peroxide, *Arch. Biochem. Biophys. 288*, 118−125.
44. Phaneuf, S., and Leeuwenburgh, C. (2002) Cytochrome *c* release from mitochondria in the aging heart: A possible mechanism for apoptosis with age, *Am. J. Physiol. 282*, R423−R430.
45. Schrader, N., Fischer, K., Theis, K., Mendel, R. R., Schwarz, G. and Kisker, C. (2003) The crystal structure of plant sulfite oxidase provides insights into sulfite oxidation in plants and animals, *Structure 11*, 1251−1263.
46. Feng, C., Kappler, U., Tollin, G., and Enemark, J. H. (2003) Intramolecular electron transfer in a bacterial sulfite dehydrogenase, *J. Am. Chem. Soc. 125*, 14696−14697.
47. Kappler, U., and Bailey, S. (2005) Molecular basis of intramolecular electron transfer in sulfite-oxidizing enzymes is revealed by high-resolution structure of a heterodimeric complex of the catalytic molybdopterin subunit and a c-type cytochrome subunit, *J. Biol. Chem. 280*, 24999−25007.
48. DeLano, W. L. (2002) *The Pymol Molecular Graphics System*, DeLano Scientific, San Carlos, CA.

BI051609L